Received: 16 July 2021 | Revised: 26 August 2021 | Accepted: 26 August 2021

DOI: 10.1002/pcr2.10208

RESEARCH ARTICLE

Polymer Crystallization WILEY

Improvement of high voltage direct current material properties upon tailoring the morphology of crosslinked polyethylenes

Christoph Felix Niedik[1] | Frank Jenau[1] | Michail Maricanov[2] | Dominik Segiet[2] | Joerg Christian Tiller[2] | Frank Katzenberg[2]

[1]Institute of High Voltage Engineering, Faculty of Electrical Engineering & Information Technology, TU Dortmund University, Dortmund, Germany

[2]Biomaterials & Polymer Science, Department of Biochemical & Chemical Engineering, TU Dortmund University, Dortmund, Germany

Correspondence
Christoph Felix Niedik, Institute of High Voltage Engineering, Faculty of Electrical Engineering & Information Technology, TU Dortmund University, D-44221 Dortmund, Germany.
Email: felix.niedik@tu-dortmund.de
Frank Katzenberg, Biomaterials & Polymer Science, Department of Biochemical & Chemical Engineering, TU Dortmund University, D-44221 Dortmund, Germany.
Email: frank.katzenberg@tu-dortmund.de

Abstract

Crosslinked linear low-density polyethylene (XLPE) is the most common polymeric cable insulation material for high-voltage applications with a high number of operating hours in high voltage alternating current (HVAC) systems. High voltage direct current (HVDC) power transmission and polymeric cable systems play a major role in the future and raise, besides numerous systemic benefits, challenges in the design of material properties. The main issue is injection and trapping of space charges in insulation materials under DC-fields. The objective of this work is to increase knowledge of the interplay between microstructure and material performance of XLPE under DC by tailoring its morphology beyond the capabilities of "common crystallization kinetics" upon constrained crystallization at certain elongations. It was found that the tailored oriented morphology influences the energetic depth of traps and a significant reduction of space charge density occurs. Moreover, the optimized oriented morphology leads to a significant reduction of field enhancement for field strengths $E_{Laplace} \geq 20$ kV mm^{-1} compared to unoriented XLPEs with spherulitic morphology. It is shown that this way of morphology tailoring results in a considerable, material dependent reduction of field exposure by a factor of 4, which promises a significant improvement in the electrical life time of polymeric insulation material used.

KEYWORDS
HVDC, morphology tailoring, polymer insulation, space charge phenomena

1 | INTRODUCTION

The energy system is in the midst of a very significant transformation. In 2030, 100% of the electricity demand has to be generated from renewable energy sources and climate neutrality has to be achieved in 2040. This requires a massive expansion of renewable energy sources and a corresponding adaptation of the electrical grid infrastructure that can continue to maintain supply security at the accustomed high level during and after this transformation process. Driven by political goals and the global increase in power demand, high-voltage-direct-current (HVDC) power transmission plays a key role in the expansion of the global high voltage power grid.

Besides stabilizing effects, like interconnecting asynchronous high-voltage-alternate-current (HVAC) grids and a controllable power exchange between HVAC networks, it allows low-loss energy transmission over long distances with technical and economic advantages. This creates opportunities to bring renewable energy generation centers into line with the existing interconnected grid, including already existing load centers. Here, polymeric cable systems replace oil-filled and mass impregnated cables and integrate renewable energy in the

form of submarine cables by connecting offshore platforms and are used in sensitive areas instead of overhead line technology for increasing acceptance of local residents.[1]

However, this technology expansion does not only lead to systemic effects, it also places new demands on the polymeric insulation materials used in the entire network equipment chain due to resultant DC fields. The requirements are manifold and a "rethinking" is necessary in comparison to design criteria chosen for AC insulation systems, since the electric field distribution in insulation materials is governed by the very low frequency electric and dielectric properties.[2]

In recent decades, polymers have been developed in many technical areas into a versatile and technically indispensable group of materials. Due to the nature of covalent bonding along the backbone and secondary bonding between the macromolecules, most polymers have low conductivity and, for this reason, they are used as insulating materials in high voltage engineering equipment. Polyethylene (PE) is the most common and studied semi-crystalline polymer with a simple hydrocarbon chain structure and is available in a variety of types and grades. Despite its rather simple structure, it is a material of high complexity, which is dependent on several material and processing conditions. Unlike most metallic and many ceramic materials, even perfect polymers without any configurative defects cannot crystallize to an extent of 100%. Thus, the microstructure of crystallizable polymers, such as PEs, cannot be rationalized in terms of a simple granular structure, but describes the arrangement of amorphous and crystalline phases, summarized under the term morphology.[3]

Dependent on density and molecular weight, polyethylenes are subdivided into different groups like low density (LDPE), linear low density (LLDPE), high density (HDPE) and ultra-high molecular weight (UHMWPE) polyethylenes. The density of any PE is linear to its crystallinity, which again depends on the number and length of branches along the macromolecular backbone. The morphology of PE crystallized from a relaxed melt basically consists of lamellae crystals, which are radially arranged to spherulitic structures. A corresponding, highly simplified schematic representation is illustrated in Figure 1.[4] In the crystalline phase, the hydrocarbon chains are aligned in planar zigzag arrays with all-trans conformation. At the lamellar surface the chains exit to either refold back into the lamella in form of a regular fold (Figure 1B) representing the amorphous-crystalline interphase, or pass through the less ordered amorphous phase and reenter the same lamella in terms of an irregular fold (Figure 1C) or enter a neighboring lamella (Figure 1E,F).[5] PE was first introduced as a cable insulation material in the United States in 1944, and in 1966 the first high-voltage AC cable with PE insulation was put into operation at a voltage of 138 kV.[6] Further improvements in the properties of PE were pursued by crosslinking the polymer through silanes, radiation or peroxides,[7] leading to a thermosetting XLPE, which allows overcoming the low melting and softening point of PE, enabling the insulation to withstand elevated operating temperatures of up to 90°C. Especially, radically crosslinked LDPE, by means of dicumyl-peroxide (DCP), was invented in 1963 and is the most common polymeric cable insulation material with a high number of operating hours rated up to 400 kV since 1988 in HVAC systems.[8] Due to the conductivity-dependent

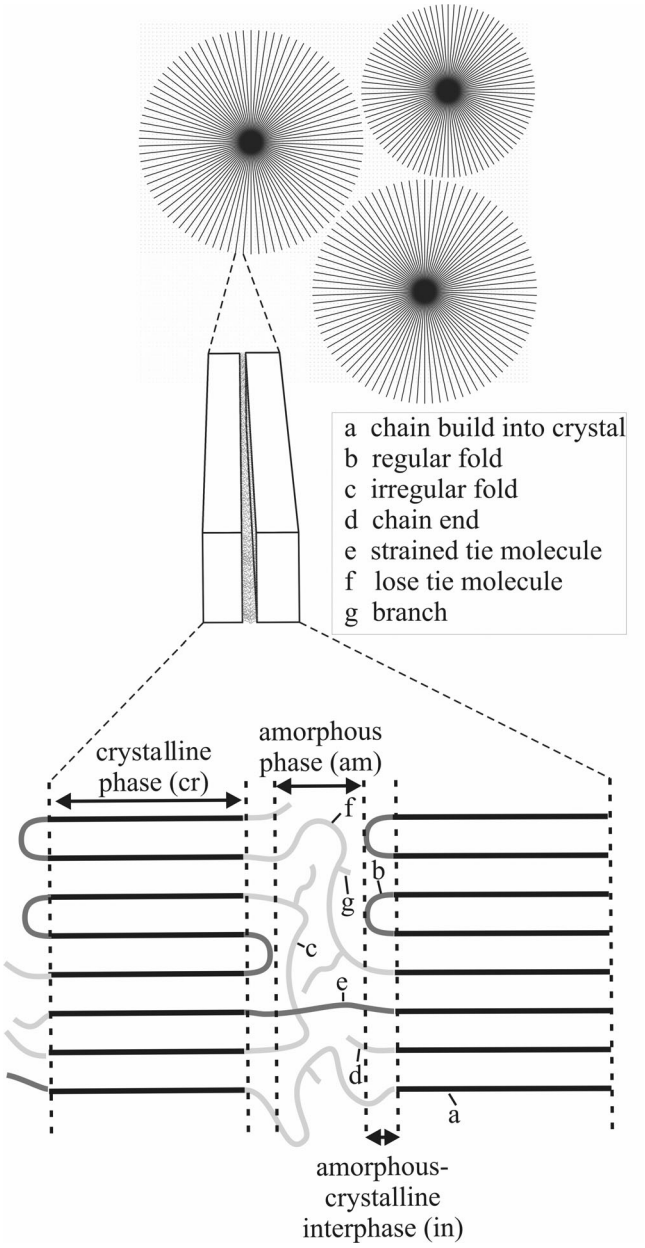

FIGURE 1 Morphology of polyethylene with its different phases based on reference[4]

electric field distribution and space charge issues in polymeric insulations under an unipolar or a reversed polarity field, the development and implementation of polymeric HVDC systems has been difficult and delayed until 1999 with the first commercial HVDC system using extruded ±80 kV cable system.[9]

A striking example of "rethinking" the suitability of crosslinked polyethylene for DC application is seen in the process step of thermal post treatment in material production, since volatile by-products created during DCP cross-linking process are possible causes for enhanced space charge accumulation, which makes a sufficient degassing of XLPE necessary before use.[10,11] But the introduction of

a cross-linking agent like DCP does not only introduce chemical bonds and by-products, it also may influence the morphology towards smaller spherulites with thinner lamellae and in case of XLPE even a reduction of the spherulitic structure or formation of lamellae stacks is reported.[12] However, besides the elimination of impurities and volatile by-products, consideration and analysis of morphology is a key element in influencing and evaluating the electrical performance of polyethylenes,[13] as microscopic and spectroscopic evidence in a variety of research papers indicate that polyethylene has a complex morphology that strongly influences charge transport and breakdown characteristics.[14] For example, if "isotropic" morphological systems are considered, it is known from studies for AC application, that significant changes of spherulite diameters influence the electrical strength.[15] With regard to general charge transport in PE, it is postulated that the wave function of the conduction band edge in PE has an interchain character, in contrast to the intrachain character of all filled valence band states. Thus, while a hole added to a neutral polyethylene will mainly belong to the polyethylene chain backbone bonds, an added electron in a polyethylene will mainly reside between the chains and far away from the existing bonds,[1] which motivates a detailed consideration of the macroscopic and microscopic, morphological characteristics.

In this context, it is known that the property of space charge accumulation is one of the most essential design criteria of polymeric insulation materials for DC application, since the buildup determines the electric field distribution under operating conditions, which may lead to accelerated aging of the material.[16–18] Various nondestructive thermal and acoustic measurement methods have been developed in the last decades to quantify the space charge distributions in insulation materials generated under DC voltage.[19,20] In this study, a pulsed electroacoustic method (PEA) is used, in which short electrical pulses are put across the insulation material stimulating existing space charges.[21] According to the Coulomb principle, forces result from the electrical pulse field, which travel through the material as acoustic waves. These waves are detected via a piezoelectric transducer and converted into an electrical signal that allows spatial quantification of the stored space charges. Since space charge phenomena are the key difference between the performance of DC and AC insulation, their suppression is an important topic in scientific research and industrial application. Approaches for suppression are the introduction of inorganic nanoparticles, grafting of functional groups and blending with other polymers, whereas morphological influences did not explicitly come into focus for active avoidance of charge accumulation. However, there are indications in many publications that morphology should play an important role in the analysis of space charge phenomena:

With regard to the influence on space charge accumulation, it was observed that the choice of the type of PE,[22] the respective configurational and morphological differences, such as molecular weight, number and length of branches, lamellae thickness and degree of crystallinity, allow a cross-correlation to the trapping and detrapping characteristics in the different materials.[21,23,24] Furthermore, it is known that above a certain electrical threshold field, field-induced morphological changes begin, which in turn have a direct influence on the charge transport in the material itself.[4] However, the formation of the semi-crystalline structure is subject to a number of thermodynamic, polymer physical and mechanical boundary conditions, which makes it challenging to adjust and forecast morphological properties in many applications. It is known that whenever a polymer is processed, a partial anisotropy of the morphology cannot be avoided.[14] For instance, during the cable manufacturing process, temperature gradients during crystallization may cause trans-crystallization zones, which in turn may cause field enhancements by location-dependent charge transport.[25,26] Or else, the pressing of the polymer melt through the extruder die may result in primarily unwanted inhomogeneous morphological effects like strain-induced orientation of molecules up to the formation of shish-kebab crystals as reported for uncrosslinked HDPE.[27–29] Also during the cable transport process, insulation is subjected to external mechanical stress due to applied bending radii, which is comparable to a cold deformation of the insulation material, involving relatively high deformation stresses and major structural changes, which may have an effect on the material structure and electrical performance.[30] Furthermore there are studies on deformation of PE showing that cold mechanical drawing leads to a decrease of structural units perpendicular to the drawing axis and therefore to a reduction of mean free path leading to an increase of electrical strength, whereas dielectric strength is decreased parallel to the drawing axis.[31] Basically, it is shown that mechanical drawing of PE in general influences amorphous and crystalline phases of the polymer affecting the electrical strength.[32,33]

Although polymer insulation materials have been used in high voltage engineering for many decades, extensive research exists to evaluate the equipment and materials used, reporting on a large number of underlying physical phenomena that affect the electrical properties of insulating materials under DC, the nature of electrical charge transport in insulating polymers is still not fully understood.[34] All research mentioned underlines the interplay of morphology and electrical properties, whereby targeted tailoring of the morphology by introducing orientation or mechanical stress and subsequent investigation of material performance under DC has not yet been the subject of intensive research work. Especially a detailed investigation of the influence of molecular as well as morphological orientation of crosslinked polyethylenes and the associated effect on space charge accumulation is currently not known and therefore subject of this publication. While crystallization of an uncrosslinked polymer in a defined oriented state upon cold drawing or calendering is hard to control due to complex relaxation processes and crazing, which makes usage under high voltage difficult, crosslinked polymers offer the advantage that their viscosity above the melting temperature remains infinite up to their decomposition. This allows stretching the polymer melt to any, freely selectable elongation, while relaxation processes are inhibited during constrained crystallization, which takes place upon cooling with a defined rate or to a defined temperature.[35–38] Thus, it is possible to take influence on the morphology, especially the orientational degree of macromolecules, the arrangement of crystalline and amorphous phases, the crystallinity, and even on thermal properties such as the melting temperature.[39,40] Summarizing, in addition to the already mentioned advantage of higher temperature

stability, cross-linking offers an efficient possibility to strongly and reproducibly influence the morphology of a thermoplastic polymer upon hot drawing above the respective melting temperature and subsequent cooling under constrained condition. Against this background, crosslinked polyethylenes were differently oriented and characterized via pulsed electro acoustic (PEA) measurements to increase knowledge of the interplay between morphology and material performance under DC fields by changing the morphology beyond the capabilities of "common crystallization kinetics."[41]

2 | EXPERIMENTAL

2.1 | Materials

Three different polyethylenes were chosen for exploring the influence of morphology on the space charge accumulation via PEA measurements:

2.1.1 | HVDC polyethylene

Polyethylene (LDPE1) is a low-density polyethylene compound based on Supercure technology, specially designed for insulation of high voltage direct current (HVDC) power cables. Since it is usually cross-linked for this application, it comes already blended with the crosslinking agent, dicumyl peroxide (DCP), in unknown concentration. The material has a density of 0.922 g m^{-3}, melt flow index of 0.2 g min^{-1} (190°C/2.16 kg), DC volume resistivity of >10^{16} Ω cm, dielectric constant of 2.3 at 50 Hz, and a dissipation factor of less than 0.0003 at 50 Hz.

2.1.2 | Lupolen 1810H

Lupolen 1810H (LDPE2) was kindly provided by Basell *Polyolefin GmbH*. It is a low-density polyethylene usually used for injection molding or blow film extrusion, having a weight average molecular weight M_w of 188 kg mol^{-1}, polydispersity of 11.3, density of 0.919 g cm^{-3}, melt flow index of 0.15 g min^{-1} (190°C/2.16 kg), and 23 branches per 1000 C-atoms, electrical resistivity of 1.00 · 10^{15} Ω cm, surface resistivity of 1.00 · 10^{14} Ohm, and dielectric constant of 2.3 at 100 Hz as well as a 1 MHz.[39,40]

2.1.3 | Vestolen 6060 A

SABIC Vestolen A 6060 (HDPE) was kindly provided by egeplast GmbH. It is a high density polyethylene with a bimodal molecular weight distribution, a weight average molecular weight of M_w = 222 kg mol^{-1}, polydispersity of 24, a density of 0.949 g cm^{-3}, melt flow index of 0.1 g min^{-1} (190°C/2.16 kg), and 2.7 branches per 1000 C-atoms.[42] Due to its long-term strength, Vestolen A 6060 is mainly used for the extrusion of pressure pipes for water, gas, and sewage.

2.2 | Sample preparation

Since LDPE1 was purchased already premixed with an unknown content of the cross-linking agent DCP, the pellets were directly compression molded in a heating press to sample plates with diameter of 160 mm and various thicknesses ranging between 0.5 and 1 mm. The samples were kept for curing in the heating press for 30 min at 160°C under exclusion of air.

In order to crosslink LDPE2 and HDPE with a degree of crosslinking preferably similar to that of LDPE1, the respective crosslinker concentration must be found prior to sample preparation. Thus, different amounts of DCP and di-tert-butyl peroxide (DTBP) were added to LDPE2 and HDPE, respectively, mixed in a twin-screw microextruder, and subsequently compression molded and cured in a heating press.

To avoid the influence of by-products on space charge formation, the obtained crosslinked LDPE (xLDPE1 and xLDPE2) and HDPE (xHDPE) were post-treated and short circuited at a temperature of 50°C in an oven for at least 3 days.[43]

2.3 | Differential scanning calorimetry

Melting temperature T_m and degree of crystallinity α_{cryst} of crosslinked polyethylenes were determined with differential-scanning calorimetry (DSC) using a DSC 2910 from TA Instruments, Inc. To this end, DSC samples with weights ranging between 10 and 20 mg were heated as well as cooled with a constant temperature rate of 10 K min^{-1}. Samples were first heated from room temperature to 160°C, then cooled to 0°C and again heated to 160°C. T_m was obtained in the peak minimum of the heat flow (exo-up). α_{cryst} was calculated from the heat of fusion ΔH_m, as determined by integration of the melting peak, by putting into relation to the equilibrium heat of fusion $\Delta H_m^0 = 289\ J\,g^{-1}$ of 100% crystalline polyethylene[44,45]:

$$\alpha_{cryst} = \frac{\Delta H_m}{H_m^0} \quad (1)$$

The absolute uncertainty of α_{cryst} is about 1.25%, basing on the standard deviation of the measurement.

2.4 | Dynamic mechanical analysis

A dynamic thermomechanical analyzer DMA (DMA 2980, TA Instruments, Inc.) was used for determination of the degree of cross-linking x_c (fraction of cross-linked repeating units) as well as to check whether the different polyethylenes are successfully crosslinked. Samples with dimensions of 10 mm x 3 mm x 1 mm (length, width, and thickness) were prepared, mounted to the film tension clamp of the DMA and analyzed up to a temperature of 200°C using a frequency of 1 Hz, an amplitude of 10 μm, a preload force of 0.01N and heating rate of 5 K min^{-1}. The samples were assumed to be cross-linked when the Young's

modulus did not change significantly upon further heating above T_m. x_c was determined according to Flory's theory of viscoelasticity.[46,47]

$$x_c = \frac{M_{rep} \cdot E(T)}{2 \cdot (1+\upsilon) \cdot \rho(T) \cdot R \cdot T} \quad (2)$$

where M_{rep} is the molecular weight of the repeating unit (28.0528 g mol^{-1}), R the universal gas constant (8.314 J mol^{-1} K^{-1}), $\rho(T)$ the density, T the absolute temperature, $E(T)$ the equilibrium storage modulus and ν the Poisson's ratio, which is assumed to be 0.5 above T_m. The equilibrium moduli were taken from the respective DMA measurements at 160°C. Since the melt density differences of the different polyethylenes are negligible, the density at 160°C was assumed for all polyethylenes as $\rho_{PE,160°C} = 0.774$ g cm^{-3} according to Flory and Orwoll.[48]

2.5 | Constrained crystallization

In order to explore the influence of morphology on the space charge accumulation in the different crosslinked polyethylenes, xLDPE1/xLDPE2 and xHDPE samples were heated to 140 and 160°C, respectively, and stretched to elongations of 2, 4, 6, 8, and 10 using a custom-made stretching apparatus. The samples were crystallized by contacting for at least 1 min a glass plate at a temperature of 80 and 100°C, respectively, before cooling to room temperature. Relevant material parameter is summarized in Table 1.

2.6 | X-ray diffraction

Small- and wide-angle X-ray scattering (SAXS, WAXS) patterns were recorded at a VANTEC-2000 detector (Bruker AXS GmbH) using a micro focus X-ray source (IμS, Incoatec GmbH) with Cu-anode and integrated Montel Optic operated at 60 kV and 0.600 mA. The X-ray wavelength was 1.5406 Å. The sample-to-detector distance was 13.25 cm for WAXS and 107 cm for SAXS. The accumulation time for each frame was 900 s. Silver behenate standard was used to calibrate the scattering angle. The parameters of the orthorhombic unit cell of polyethylene are $a = 0.417$ nm, $b = 0.4945$ nm, $c = 0.2547$ nm.

2.7 | Space charge measurements

The space charge characteristics in crosslinked polyethylene are measured by the pulsed-electroacoustic (PEA) method as schematically depicted in Figure 2.[21] Therefore, polymeric test material is exposed to a DC field

TABLE 1 Crosslinker concentration c, extrusion temperature T_{ext} and time t_{ext}, curing temperature T_{cur} and time t_{cur}, and resulting degrees of crosslinking x_c of the different PEs

	c_{DCP} [wt%]	c_{DTBP} [wt%]	T_{ext}/t_{ext} [°C/min]	T_{cur}/t_{cur} [°C/min]	x_c [%]
xLDPE1	a	-	-/-	180/20	0.23
xLDPE2	0.5	-	116/5	180/20	0.22
xHDPE	-	0.27	160/-	160/90	0.30

[a]DCP content unknown.

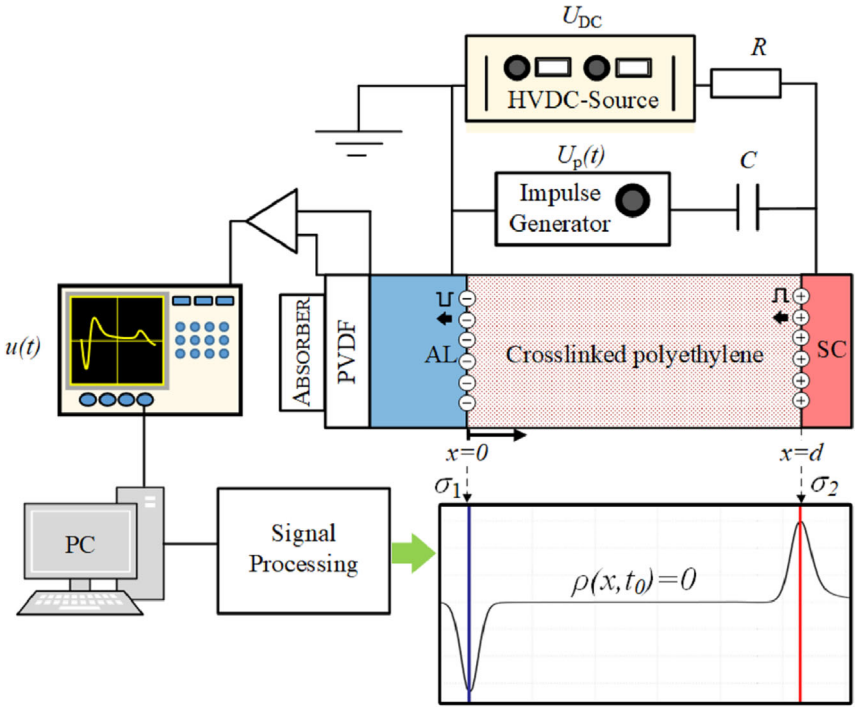

FIGURE 2 Pulsed electroacoustic method measurement setup

between high voltage (HV) and ground electrode made of aluminum (AL). For the purpose of acoustic impedance matching conductive compound, so called "semicon" (SC) material is used as HV electrode. The setup consists of external components in terms of a Spellman SL150PN1200 DC power supply (0–150 kV, 8 mA), a Tektronix DPO 5034B digital oscilloscope and fletcher type impulse generator with a repetition rate of 150 Hz and a pulse width of 5 ns. The detection of pressure waves in the PEA cell and transformation into voltage signal is conducted using a 9 μm piezoelectric polyvinylidene fluoride PVDF transducer. The measured time dependent voltage signal $u(t)$ is converted into a space charge signal $\rho(x, t_{\mathrm{HVon,HVoff}})$ according to technical specification.[49] Based on a space-charge free sample ($\rho(x, t_0) = 0$), the application of DC voltage U_{DC} only leads to surface charges σ_1 and σ_2. Therefore, deconvolution of measured signal is performed using spectral division with additional Gaussian filtering using a cut-off frequency of 25 MHz, and no correction of material specific attenuation and dispersion is done. For the purpose of comparability of different measuring procedures, an automated measurement software is used. Test samples are loaded dynamically with DC field strengths of $E_1 = 10\ \mathrm{kV\,mm^{-1}}$, $E_2 = 20\ \mathrm{kV\,mm^{-1}}$, $E_3 = 30\ \mathrm{kV\,mm^{-1}}$, and $E_4 = 40\ \mathrm{kV\,mm^{-1}}$ for $t_{\mathrm{HVon}} = 7200$ s followed by HV-Off-phase for at least $t_{\mathrm{HVoff}} = 3600$ s.

2.8 | Determination of permittivity

LCR-Meter HP 4284A in combination with electrode arrangement 16451B is used to determine the capacity C_{PE} of the test objects in a frequency range from 20 Hz to 1 MHz. Measurements are performed in electrode contacting mode with a test voltage of 20 V and capacity results are averaged over frequency range. The permittivities ε_{r}, needed for PEA analysis, are calculated using the average thickness of test material d_{PE}, area of guarded electrode A and dielectric constant ε_0:

$$\varepsilon_{\mathrm{r}} = d_{\mathrm{PE}} C_{\mathrm{PE}} / A \varepsilon_0 \tag{3}$$

3 | RESULTS AND DISCUSSION

The objective of this study was to explore the influence of morphological changes and aspects on the space charge accumulation in crosslinked polyethylenes under DC.

3.1 | Microstructural characterization

To this end we chose a low-density polyethylene (LDPE1) especially synthesized for high voltage DC power cables, Lupolen 1810H (LDPE2), a low-density polyethylene commonly used for injection molding or blow film extrusion, and Vestolen A 6060 (HDPE), a high-density polyethylene commonly used for extrusion of pressure pipes.

While LDPE1 is already composed with an unknown content of crosslinking agent and, thus, can be directly compression molded to test sheets, LDPE2 and HDPE still had to be crosslinked to a degree of crosslinking preferably similar to that of LDPE1. To this end, we chose DCP and di-tert-butyl peroxide (DTBP) as crosslinker for LDPE2 and HDPE, respectively, prepared a series of samples using different crosslinker concentrations c, and determined the resulting degrees of crosslinking x_{c} from the Young's modulus at 160°C according to Flory's theory of viscoelasticity. The respective Young's modulus versus temperature plots of crosslinked xLDPE1 and similarly crosslinked xLDPE2 and xHDPE samples are shown in Figure 3.

The degree of crosslinking x_{c} of xLDPE1 was determined to 0.22%. We were capable of realizing a nearly similar x_{c} of 0.23% for xLDPE2 by applying a DCP concentration of 0.5 wt% and a slightly higher x_{c} of 0.30% for xHDPE by applying a DTBP concentration of 0.27 wt% (Table 1). Using smaller concentrations unfortunately did not render the HDPE into an elastomeric network and results in irreversible deformation upon stretching in the molten state. Possible reasons for this might be the smaller number average molecular weight ($M_{\mathrm{n}} = M_{\mathrm{w}}/\mathrm{PDI}$) as well as the smaller degree of branching of HDPE in contrast to LDPE1 and LDPE2.

The degrees of crystallization α_{CRYST} and melting temperatures T_{m} of the crosslinked polyethylenes were determined by DSC (see Table 2).

In order to explore the influence of the structural and morphological orientation on the space charge accumulation, the three polyethylene networks were crystallized under constrained condition. To this end, samples of xLDPE1/2 and xHDPE were heated to 140 and 160°C, respectively, and stretched to elongations λ ranging from 2 to 10. In order to crystallize under constrained condition, the strain was kept constant while the samples were rapidly cooled to an isothermal crystallization temperature by

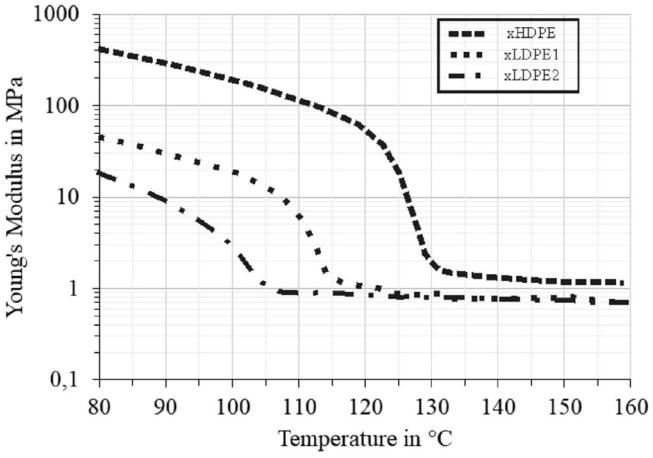

FIGURE 3 Young's modulus versus temperature plots

TABLE 2 Degrees of crosslinking x_{c} and crystallinity α_{cryst}, and melting temperatures T_{m} of PE networks

Sample	x_{c} [%]	α_{crys} [%]	T_{m} [°C]
xLDPE1	0.22	35.5	109.6
xLDPE2	0.23	31.2	101.5
xHDPE	0.30	70.8	129.7

bringing in contact to an appropriately heated glass plate for at least 1 min. For xLDPE1/2 and xHDPE samples the isothermal crystallization temperatures were chosen as 80 and 100°C, respectively. Finally, the samples were cooled to room temperature.

The differently constrained crystallized PEs were microstructurally characterized by WAXS experiments to determine the orientational order of crystals as well as of macromolecular chains in the amorphous phase and by SAXS to gain information about morphological aspects. Figure 4 representatively shows SAXS and WAXS diffraction patterns as well as schemes of the respective morphology of relaxed and differently constrained crystallized xLDPE1.

A biaxial crystalline orientation precessing around the direction of applied strain during constrained crystallization was found for all crosslinked PEs. As indicated by the (110) reflections, the deviation φ of these two preferential orientations from the stretching direction becomes smaller with increasing stretching ratio and converges to a purely uniaxial orientation at a λ of at most 8 for the xLDPEs and 6 for xHDPE. The crystalline degree of orientation O_{cryst} was calculated from the full width at half maximum of the equatorial (110) reflections of the polyethylene crystals along the azimuthal direction χ (see Figure 5) using the following equation[50]:

$$O_{cryst} = \frac{180^\circ - \Delta\chi}{180^\circ} \tag{4}$$

The orientation of chains along the stretching direction in the amorphous phase was evaluated using the peak scattering intensities of the amorphous halos at the equator $I_{a,equator}$ and meridian $I_{a,meridian}$ of the diffraction patterns. The degree of orientation of chains in the amorphous phase O_{amorph} was determined using[51]:

$$O_{amorph} = \frac{I_a(\text{equator}) - I_a(\text{meridian})}{I_a(\text{equator})}. \tag{5}$$

Figure 6 shows the degrees of orientation of crystals O_{cryst} and macromolecular chains in the amorphous phase O_{amorph} for

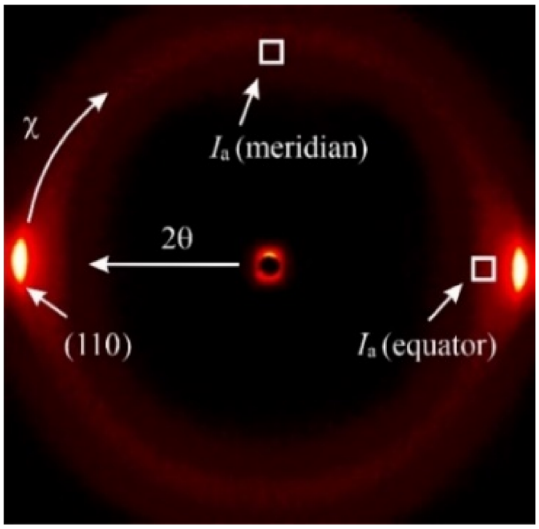

FIGURE 5 Representative WAXS diffraction pattern of crosslinked LDPE1, crystallized at an elongation of $\lambda = 10$

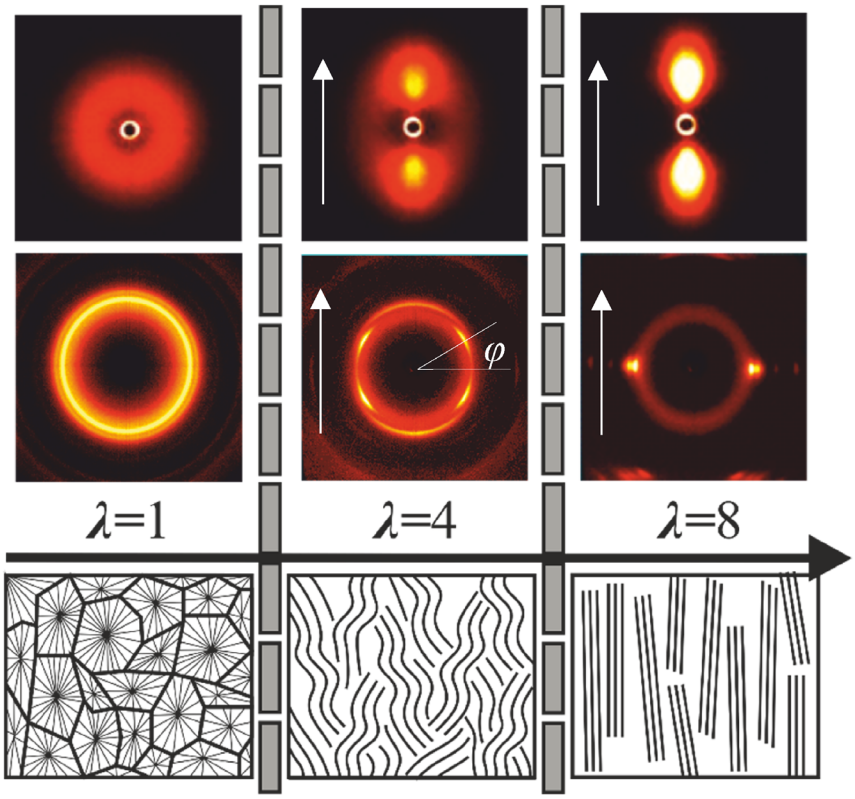

FIGURE 4 SAXS (top) and WAXS (middle) diffraction patterns of xLDPE1, constrained crystallized at different elongations λ, and respective schemes of the morphology, deduced from diffraction patterns (bottom). Arrows indicate the direction of strain applied during crystallization

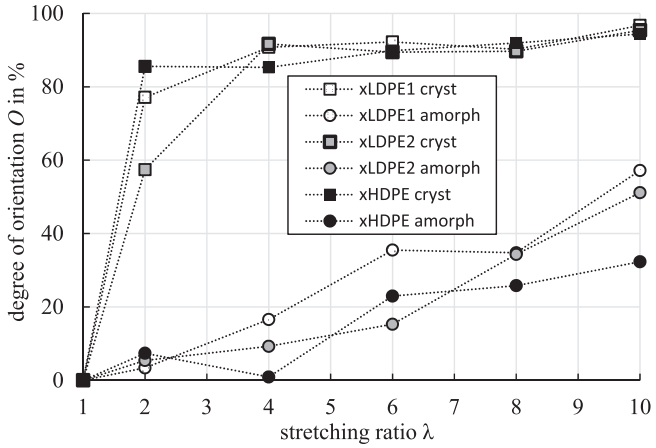

FIGURE 6 Crystalline and amorphous degree of orientation of xLDPE1, xLDPE2, and xHDPE in dependence on stretching ratio λ

xLDPE1, xLDPE2 and xHDPE in dependence on the elongation applied during crystallization. While O_{cryst} increases sharply to values around 90% with increasing stretching ratio, O_{amorph} increases gradually with increasing λ. Assuming a lamellae crystalline morphology, this indicates that constrained crystallization even at small stretching ratios results in a highly oriented morphology with lamellae aligned under $90° \pm \varphi$ to the stretching direction during crystallization.

3.2 | Space charge accumulation

3.2.1 | Trapping properties

The evolution of space charge accumulation during HVon-phase was characterized by spatially resolved analysis of measured space charge density over time for all crosslinked PEs, crystallized at elongations λ ranging from 1 to 10. For the sake of overview, Figure 7 exemplarily depicts the measurement results for unstretched as well as at $\lambda = 8$ crystallized xLDPE1, xLDPE2, and xHDPE. The unoriented crystallized xLDPE1 and xLDPE2 in Figure 7A,C shows dominant accumulation of positive charges $\rho(x, t = 7200s)$ on the anode side and in the bulk reaching up to the counter electrode, as indicated by the curve above the abscissa. Due to the resulting mirror charge, the measured height of positive charge carriers at the positive electrode is consequently reduced. In contrast to this, the charge accumulation in unoriented xHDPE in Figure 7E shows considerably less trapping behavior. According to the literature, this is assumed to correspond to the basic linkage of charge transport and morphology of PE, since trapping is reduced with increasing crystallinity.[23,24,52]

Crystallization of PE under constrained conditions changes the space charge characteristics. Both oriented xLDPE's show an obvious change and reduction of positive trapping characteristic in the bulk with a lower total number of space charge accumulation with increasing stretching ratios, as depicted in Figure 7B,D for a stretching ratio of $\lambda = 8$. In addition, a slight near-electrode extension of the trapping zone is evident. This trapping zone is wider in xLDPE1 than in xLDPE2. This effect also occurs for oriented xHDPE as shown in Figure 7F, but in addition stretching ratios $\lambda \geq 2$ lead to a slight increase of charge injection and accumulation, and, thus, a tendency to deterioration of the electrical performance.

3.2.2 | Application view: Field enhancement factor

According to Poisson's equation, trapped space charge accumulation in an insulation material leads to local field enhancements

$$E(x, t_{HVon}) = -\int_0^d \frac{\rho(x, t_{HVon})}{\varepsilon_0 \varepsilon_r} dx, \tag{6}$$

which in turn have an influence on service life of the equipment. In the case when a DC cable is installed in transmission networks with Voltage-Source-Converter-Technology (VSC-Technology), life of cable insulation is approximated by inverse-power-law.[53] Following Cigré recommendations for testing of extruded cables systems, a field enhancement of 10% reduces the service life by a factor of about 3.[54] Therefore, from the application point of view, the knowledge of field enhancement factor (FEF) occurring during operation is an essential valuation parameter:

$$\mathrm{FEF}(E_{i_{Laplace}}) = \frac{E_{i\max} - E_{i\,Laplace}}{E_{i\,Laplace}} \wedge i = \{1,2,3,4\} \tag{7}$$

$E_{i_{max}}$ represents maximum electric field during corresponding applied Laplace-field $E_{i_{Laplace}}$. Figure 8 shows exemplarily field distributions in xLDPE1 with stretching ratios of $\lambda = 1$ and $\lambda = 8$.

It is shown that the orientation of the xLDPEs have a positive influence on the performance under DC, as it leads to a reduction of the space charge-induced field enhancements.

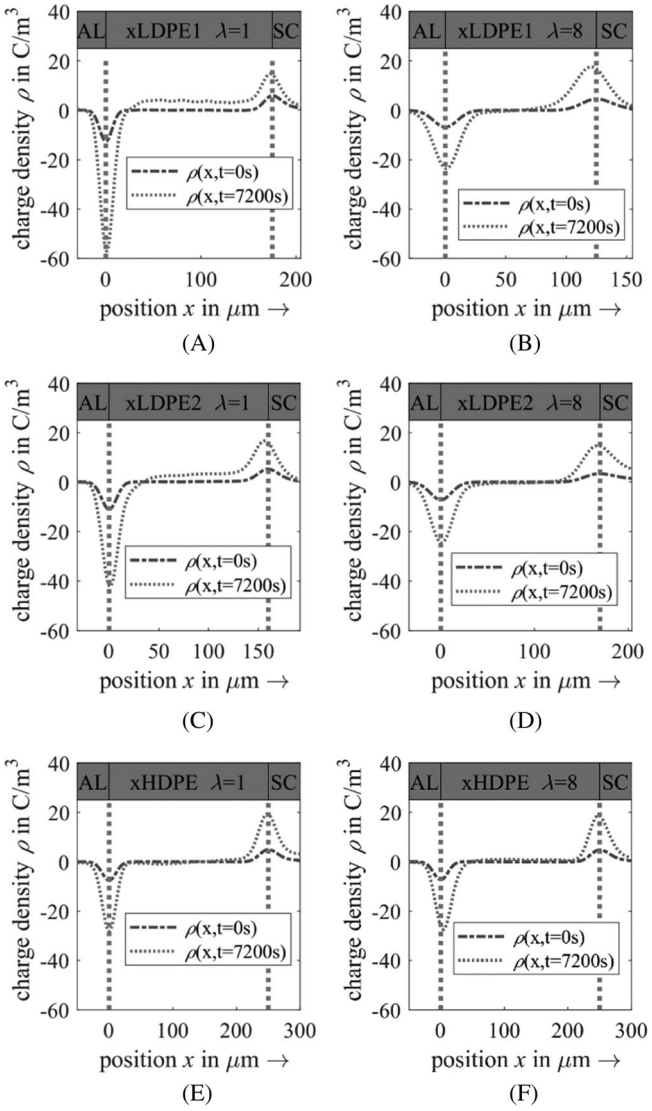

FIGURE 7 Space charge densities in xLDPE1 (A, B), xLDPE2 (C, D), and xHDPE (E, F) at the beginning and end of HVOn-phase

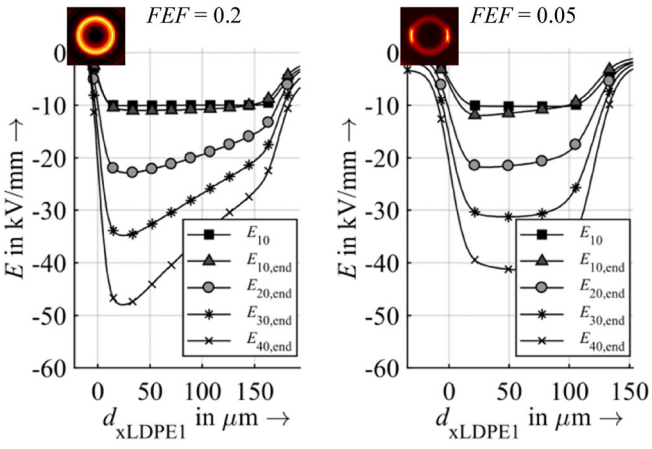

FIGURE 8 Space charge dependent distribution of electrical field in xLDPE1 for $\lambda = 1$ (left) and $\lambda = 8$ (right)

3.2.3 | Detrapping properties

Besides the trapping characteristic and resulting field situation, experimental investigation of detrapping characteristic is promising to identify microstructural information of polymeric insulation material. To this end, material specific detrapping of space charges was analyzed with a two-level detrapping model according to reference.[55] Therefore, determination of total amount of space charge over time during HVoff-phase was carried out by

$$Q_{\mathrm{HVoff}}(t) = A\int_0^d |\rho(x, t_{\mathrm{HVoff}})|dx, \tag{8}$$

where the value range of x ranges between the electrode positions 0 and d, A is the electrode area and induced charges on the electrodes are not taken into account. The number density of trapped charge over time $n(t)$ was determined by dividing the total amount of space charge by the electrode area, material thickness and elementary charge. The resulting decay behavior was approximated by two discrete trap levels after switching off the DC field:

$$n(t) = \frac{Q_{\mathrm{HVoff}}(t)}{A\,d\,e} = n_{\mathrm{st}}\exp(-k_{\mathrm{st}}t) + n_{\mathrm{dt}}\exp(-k_{\mathrm{dt}}t), \tag{9}$$

where n_{st} and n_{dt} represent the number density of trapped charges in shallow and deep traps at the moment when the applied field is removed, and k_{st} and k_{dt} are the thermal detrapping rate constants of shallow and deep traps, which are potentially related to material specific microstructure.[41] Figures 9 and 10 show the charge detrapping processes and fitting results according to the two-level decay model in xLDPE1 and xLDPE2 in dependence on the stretching ratio. The coefficient of determination of the fitted results is between $0.97 \le R^2 \le 0.99$. The measurement results support the visual observations of trapping characteristics in Figure 7.

Therefore, a reduction of number density of trapped charge is achieved by increasing of λ. In the case of the xLDPE1, it can be seen that the reduction of the space charge starts for a stretching ratio of $\lambda \ge 4$, wherein xLDPE2 exhibits a direct reduction in charge storage with increasing stretching ratio. Considering the absolute values of coefficients n_{st} and n_{dt}, it is evident that the total number of trapped charges in shallow and deep traps decreases for both LDPEs up to a magnitude of 83% in case of xLDPE1 and up to 87% in case of xLDPE2. Corresponding results for thermal detrapping rates are depicted in Figure 11.

For both materials, it is shown that crystallization under stretched conditions results in a significant change of thermal detrapping rates. In general, it is seen that orientation leads to an increase of detrapping rates of shallow and deep traps in all cases.

In contrast to xLDPEs, the number density of trapped charge in xHDPE increases with increasing stretching ratio λ as depicted in Figures 12 and 13A. It is particularly noticeable that the number density of deep trapped charges is significantly increased by orientation. Moreover, in line with the attitude of expectation for samples with

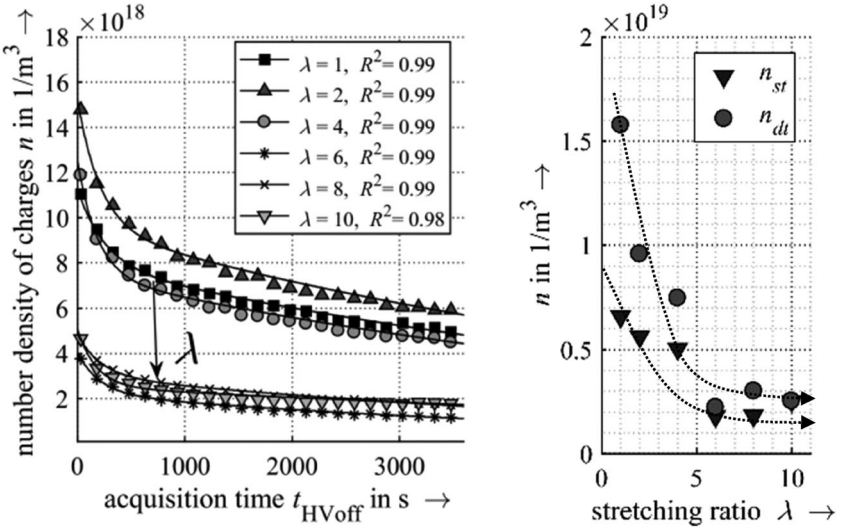

FIGURE 9 Number density of trapped charges over time using two-level detrapping model for xLDPE1

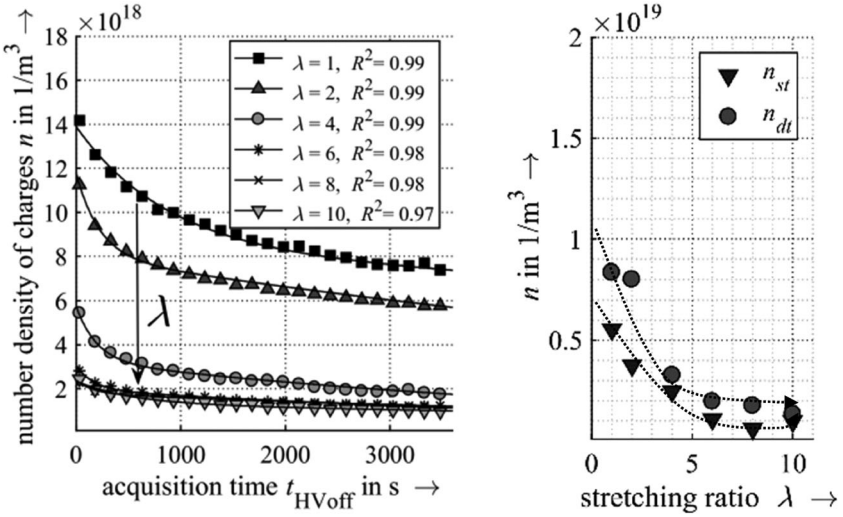

FIGURE 10 Number density of trapped charges over time using two-level detrapping model for xLDPE2

higher molecular weight,[24] the thermal detrapping rate k_{dt} in Figure 13B is substantially lower for unstretched xHDPE in comparison to xLDPE's and fluctuates with raised elongation.

3.3 | Correlation between microstructure and space charge accumulation

As already indicated, linear as well as crosslinked PEs are known to commonly crystallize in form of lamellae that, in case of an unoriented relaxed melt, arrange themselves into spherical supermolecular structures, referred to as spherulites. Although a spherulitic morphology principally offers, especially in case of large spherulites, micro-scaled, highly oriented areas, nearly all properties are quasi-isotropic at the macroscopic scale. With increasing orientational order of the melt during crystallization, PE forms stacked lamellae morphologies with increasing degrees of crystalline and amorphous orientation, as well as increasing macroscopic anisotropy. Crosslinking a linear polymer opens up the possibility to reproducibly adjust the orientational degree of the melt and, thus, to take a stronger control on morphology upon constrained crystallization.[40]

As shown in Figure 6, the degrees of crystalline and amorphous orientation increase with increasing elongation λ during crystallization. While the chain orientation in the crystalline phase increases rapidly and keeps nearly constant above $\lambda = 4...6$, the orientation of chains in the amorphous phase increases slightly and continuously with increasing λ. According to Figures 9–11 and 13, it is visible that this orientation of the amorphous and crystalline phases influences the energetic depth of the traps. In order to quantify this influence, corresponding depths of shallow (E_{st}) and deep traps (E_{dt}) were calculated using the following equation[55]:

$$E_{st,dt} = kT\ln\left(\frac{N_C v_{th}\sigma_c}{k_{st,dt}}\right), \quad (10)$$

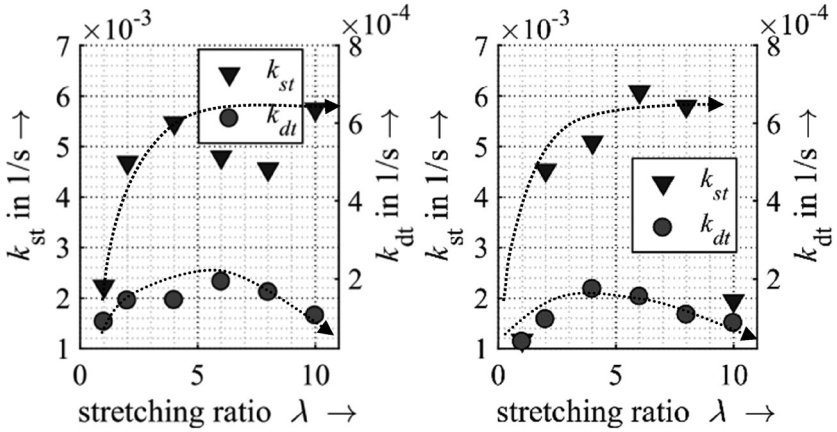

FIGURE 11 Number density of trapped charge and thermal detrapping rate constants for shallow and deep traps in xLDPE1 and xLDPE2

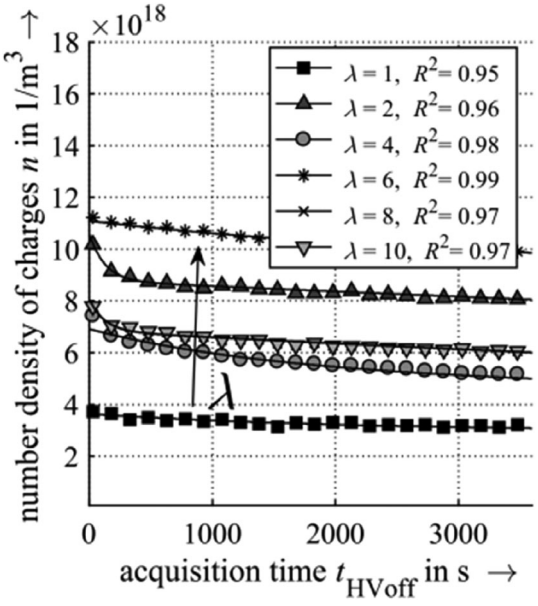

FIGURE 12 Approximation of number density of trapped charges over time using two-level detrapping model for xHDPE

where k is the Boltzmann constant, T is the temperature, $N_C = 2\left(\frac{2\pi m_e kT}{h^2}\right)^{3/2}$ is the effective density of states in the conduction band, $v_{th} = \left(\frac{3kT}{m_e}\right)^{\frac{1}{2}}$ is the thermal velocity of charge, $\sigma_c = 1 \cdot 10^{-18}$ m^2 the capture cross section of the trapping center, h is Plank's constant and m_e is the electron mass. A detailed description of the calculation method can be found in [10.1063/1.3273491] [Quelle 55]. Corresponding mean values $E_{st,\mu}$, $E_{dt,\mu}$, maximum values $E_{st,max}$, $E_{dt,max}$ (for unstretched materials, $\lambda = 1$) and highest reduction of trap depths due to orientation $E_{st,min}$, $E_{dt,min}$ are summarized in Table 3. It can be seen that the crystallization of xLDPE materials from an oriented melt leads on average to a reduction of the shallow and deep traps and, thus, implies a general potential for the adjustment of the electrical properties of PE. In the case of xHDPE, this effect is only observed for the deep traps, which may be related to the fundamentally lower proportion of mobile amorphous phase. However, these results show that the material property in terms of shallow and deep trap depth is significantly influenceable upon tailoring the morphology of xLDPEs by crystallization in a defined oriented state and motivate further consideration of the interplay between morphology and electrical performance.

Basically, trapping results in Figure 7 are in accordance to experimental evidence[56,57] of investigation of space charge accumulation in LDPE with AL and SC electrodes. In this case of electrode conformation, positive charge transport predominates in PE. Positive holes at the anode are initiated by extraction of electrons, which travel along the polymer chain to the counter electrode. On this way, it is assumed that they are hindered by amorphous phase structures in terms of folds and kinks and positive trapping occurs.[56] According to literature, boundaries of spherulites or respectively crystalline-amorphous interphases are seen as trapping centers blocking up the transportation of space charges.[58] Combining the microstructural information of the xLDPE's with the findings regarding the space charge dependent distribution of electrical field and the trapping/detrapping characteristics (Figures 7–11) allows the consideration and evaluation of a general property change: It is obvious that orientation is capable of minimizing the accumulation of charge carriers in xLDPE. A hypothesis for explanation is formed by the approach of microstructural change and optimization of amorphous-crystalline microstructure according to the schematic model in Figure 4. According to previous results in Figures 9 and 10, we assume that an optimized morphology develops when xLDPE is crystallized above a threshold-stretching ratio of λ_{thresh}. Thus, the observed decreasing space charge densities with increasing stretching ratio can be explained by growing anisotropy and formation of a stacked lamellae morphology, which leads to a decreasing electric field component normal to the crystalline-amorphous interphases. The tailoring of the morphology by aligning crystalline and amorphous phases to a stacked lamellae structure implicitly leads to an elimination of the spherulitic interfaces in the material, which is a further evidence supporting the hypothesis to explain the reduced density of trap centers.

Considering this threshold value λ_{thresh}, for the application view it is shown that an optimized orientation significantly reduces field

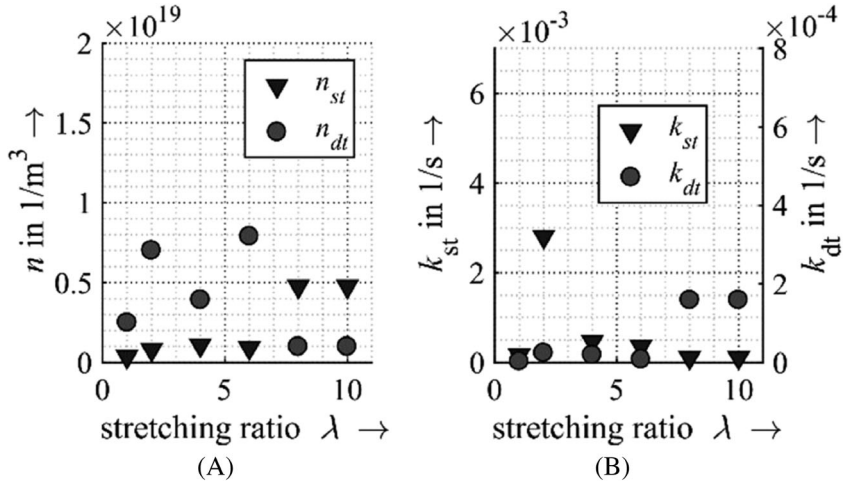

FIGURE 13 Number density of trapped charge and thermal detrapping rate constants for shallow and deep traps in xHDPE

TABLE 3 Possible reduction of trap depth by crystallization of orientated melt

Sample	$E_{st,max}$ ($\lambda = 1$) [eV]	$E_{st,\mu}$ [eV]	$E_{st,min}$ [eV]	$E_{dt,max}$ ($\lambda = 1$) [eV]	$E_{dt,\mu}$ [eV]	$E_{dt,min}$ [eV]
LDPE1	0.998	0.971	0.965	1.066	1.056	1.047
LDPE2	0.964	0.936	0.922	1.034	1.01	0.995
HDPE	0.93	0.931	0.93	1.239	1.211	1.193

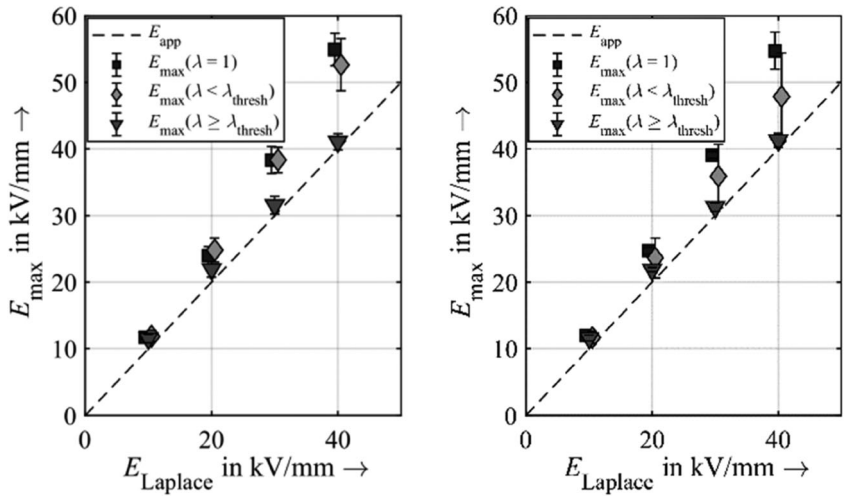

FIGURE 14 Maximum electric field enhancement under DC field conditions in xLDPE1 and xLDPE2

enhancement under DC stress. For validation, further measurements were carried out.

Figure 14 depicts the trapping characteristic by statistically analyzed maximum electric fields with different electrical field strengths for unoriented and oriented xLDPE. It can be seen that an optimized oriented morphology ($\lambda \geq \lambda_{thresh}$) leads to a significant reduction of field exposition for field strengths $E_{Laplace} \geq 20$ kV mm^{-1} in comparison to xLDPEs with spherulitic structure crystallized from relaxed melt. An increase in crystallinity alone seems unlikely for the reduction of trapping since oriented crystallization only marginally affects crystallinity. Thus, we hypothesize the orientation of the crystalline, amorphous and especially the amorphous-crystalline interphase in combination with reduction of spherulitic interfaces as responsible for the observed effects in the trapping characteristics.

The observed xLDPE detrapping behavior is analyzed and explained microstructurally as follows: Detrapping in PE is basically postulated as a function of molecular weight.[24] In the case of xHDPE, it seems likely that this dependence correlates more likely with the number of end groups than the length of the macromolecules and, thus, with a fundamentally lower number of dangling ends in the amorphous phase. An extension of this explanatory approach is the consideration of amorphous phase and orientation as essential evaluation criterion to influence the energetic depth of traps. Focusing the amorphous characteristic of xLDPE leads to the physical interpretation of high mobility, caused by the molecular degree of freedom in terms of branches, lose tie molecules and chain ends according to

Figure 15. In this model, it is assumed that this part of microstructure is conducive for emptying of traps located in the amorphous-crystalline-interphase. Considering the course of the detrapping rate in Figure 11 and Table 3, a microstructural potential for optimizing trap depths by orientation during crystallization in xLDPE is identified.

A validation of this model idea of microstructure/space charge accumulation relationship can be found by taking a closer look on the material performance of unoriented and oriented crystallized xHDPE. Unoriented xHDPE has a lower mobility and deeper traps due to larger crystals, lower surface to volume ratio and correspondingly fewer amorphous volume fraction.

Therefore, it is assumed that the trapping characteristic in xHDPE raises with increasing orientation, since the already lower amount of mobile amorphous phase in comparison to xLDPE is the more sterically hindered the more the ratio of strained- to loose-tie molecules increases with orientation and, thus, the dynamic of the amorphous phase converges against that of the amorphous-crystalline interphase.[59] This increase in the phase leads to an increased number of trapping centers in the model idea. To support this hypothesis, further measurements were carried out on unoriented and oriented xHDPE. Statistically evaluated results are depicted in Figure 16 and show that material samples with $\lambda > 1$ generally exhibit increased trapping behavior. Therefore, orientation of xHDPE deteriorates the performance under DC. Furthermore, any loose-tie molecules that are present in xHDPE become strained-tie molecules and, due to the lack of branches, detrapping must be inhibited with increasing orientation, which basically prevents the possibility of microstructural influence on the depths and densities of deep traps.

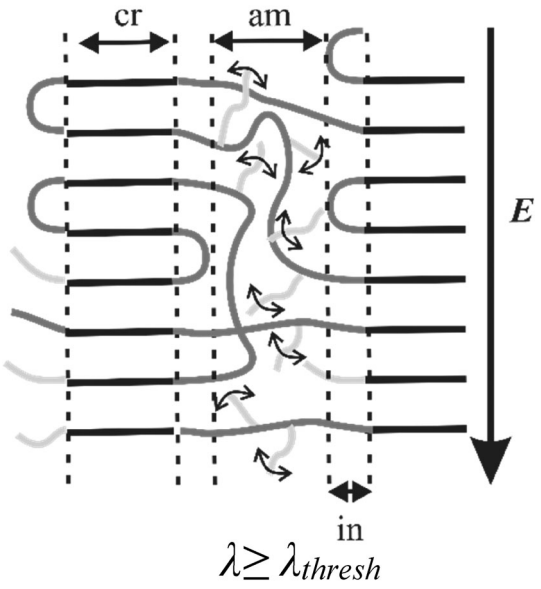

FIGURE 15 Interaction of applied field and crystalline, amorphous and amorphous-crystalline interphase of tailored xLDPE with stretching ratios $\lambda \geq \lambda_{thresh}$ (cr = crystalline, am = amorphous, in = interphase)

4 | CONCLUSION AND OUTLOOK

The objective of this work was to increase knowledge of the interplay between morphology and material performance under DC fields by changing the morphology, specifically the orientation, beyond the capabilities of "common crystallization kinetics." To this end, three different polyethylenes were crosslinked to nearly the same degree, hot-drawn above their melting temperature to different elongations and subsequently crystallized under constrained condition. As expected from a polymer physics point of view, the orientation of macromolecules in the crystalline and amorphous phases increase with increasing elongation applied during crystallization. It was found that this orientation takes influence on the energetic depth of traps and a significant reduction of space charge density occurs. Moreover, it can be stated that an optimized oriented morphology ($\lambda \geq \lambda_{thresh}$) leads to a significant reduction of field enhancement by a factor of 4 for field strengths $E_{Laplace} \geq 20$ kV mm^{-1} for both investigated xLDPEs in contrast to unoriented xLDPEs with spherulitic morphology. We hypothesize the orientation of the crystalline, amorphous and especially the amorphous-crystalline interphase in combination

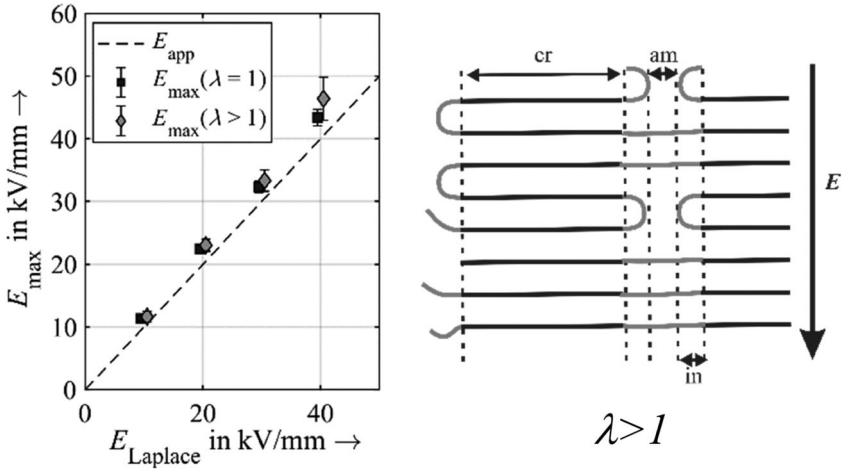

FIGURE 16 Maximum electric field enhancement under DC field conditions in xHDPE and interaction of resultant morphology by stretching ratios $\lambda > 1$ and applied electric field

with an elimination of spherulitic boundaries as responsible for the observed effects in the trapping characteristics and field enhancements. The high mobility in the amorphous phase of xLDPEs according to branches, loose-tie molecules and chain ends is assumed to be conducive for emptying of traps located in the amorphous-crystalline interphase, while the orientation along field direction seems to play a significant role regarding the transportation of electrons and holes through the material. Despite of the necessity to answer on many scientific and technological questions, such as the validation of the here described beneficial effects for application-near cable geometric setups, it can be already concluded that tailoring the morphology of polyethylenes offers great potential to suppress space charge accumulation in xLDPEs. The described findings reveal synergy effects through an interdisciplinary analysis, open up a new approach of material design for application in polymeric cable systems, should be further investigated in the future and were already filed for patent.[60]

ACKNOWLEDGMENTS

The authors thank Jens Mathiak for permittivity measurements and xLDPE2 sample preparation.

Open access funding enabled and organized by Projekt DEAL.

ORCID

Frank Katzenberg https://orcid.org/0000-0001-6585-5534

REFERENCES

[1] S. Wang, in *Polymer Insulation Applied for HVDC Transmission* (Ed: B. Du), Springer Singapore, Singapore **2021**, p. 3.
[2] A. Kuchler, *High Voltage Engineering: Fundamentals - Technology – Applications*. Berlin, Heidelberg, Springer Vieweg; **2018**. https://doi.org/10.1007/978-3-642-11993-4
[3] U. W. Gedde, *Polymer Physics*, Kluwer Academic Publishers, Dordrecht **1995**.
[4] J. P. Jones, J. P. Llewellyn, T. J. Lewis, *IEEE Trans Dielectr Electr Insul* **2005**, *12*, 951.
[5] P. J. Flory, *J Am Chem Soc* **1962**, *84*, 2857.
[6] E. Peschke, R. von Olshausen, *Cable Systems for High and Extra-High Voltage: Development, Manufacture, Testing, Installation and Operation of Cables and Their Accessories*, Berlin, Wiley VCH, **1999**.
[7] M. Lazár, R. Rado & J. Rychlý, Polymer Physics: Crosslinking of Polyoelfins, Springer, Berlin, Heidelberg, **1990**, 149.
[8] F. Precopio, *IEEE Electr Insul Mag* **1999**, *15*, 23.
[9] S. Dodds, K. Akman, B. Jacobson, T. Worzyk, A. Ab & S. Nilsson, HVDC VSC (HVDC light) Transmission - Operating Experiences, **2010**.
[10] T. Kato, R. Onozawa, H. Miyake, Y. Tanaka, T. Takada, *Electr Eng Jpn* **2017**, *198*, 19.
[11] T. L. Hanley, R. P. Burford, R. J. Fleming, K. W. Barber, *IEEE Electr Insul Mag* **2003**, *19*, 13.
[12] U. H. Nilsson, R. C. Dammert, A. Campus, A. Sneck, H. Jakosuo-Jansson, ICSD'98. Proceedings of the 1998 IEEE 6th International Conference on Conduction and Breakdown in Solid Dielectrics (Cat. No.98CH36132), **1998**, 365.
[13] P. J. Phillips, *IEEE Trans Electr Insul* **1978**, *13*, 69.
[14] R. Bartnikas, R. M. Eichhorn, *Engineering Dielectrics Volume IIA: Electrical Properties of Solid Insulating Materials: Molecular Structure and Electrical Behavior*, American Society for Testing and Materials, Philadelphia, PA **1983**.
[15] I. L. Hosier Doctoral Thesis, University of Reading, **1996**.
[16] G. Mazzanti, G. Montanari, *IEEE Trans Dielectr Electr Insul* **2005**, *12*, 876.
[17] R. J. Fleming, *Braz J Phys* **1999**, *29*, 280.
[18] C. F. Niedik, F. Jenau, *VDE-Hochspannungstechnik 2016 - ETG-Fachtagung*. Berlin, VDE Verlag; **2016**, p. 6.
[19] P. Morshuis, M. Jeroense, *IEEE Electr Insul Mag* **1997**, *13*, 26.
[20] Y. Li, T. Takada, *IEEE Electr Insul Mag* **1994**, *10*, 16.
[21] C. F. Niedik, F. Jenau, IEEE 2nd Int. Conf. Dielectrics (ICD), **2018**, 1.
[22] G. C. Montanari, G. Mazzanti, F. Palmieri, A. Motori, Proc. 2001 IEEE 7th Int. Conf. Solid Dielectrics, **2001**, 240.
[23] T. Mizutani, Ann. Rep. Conf. Electr. Insul. Dielectric Phenomena, **2006**, 1.
[24] B. Vallayer, P. Hourquebie, D. Marsacq, H. Janah, Conf. Record 1996 IEEE Int. Symp. Electr. Insul, **1996**, 674.
[25] J. Muccigrosso, P. J. Phillips, *IEEE Trans Electr Insul* **1978**, *EI-13*, 172.
[26] P. Carstensen, A. A. Farkas, A. Campus, U. H. Nilsson, *Ann. Rep. Conf. Electr. Insul. Dielectr. Phenom.* **2005**, *2005*, 381.
[27] I. L. Hosier, D. C. Bassett, I. T. Moneva, *Polymer* **1995**, *36*, 4197.
[28] J. A. Pople, G. R. Mitchell, S. J. Sutton, A. S. Vaughan, C. K. Chai, *Polymer* **1999**, *40*, 2769.
[29] F. H. Moy, M. R. Kamal, *Polym Eng Sci* **1980**, *20*, 957.
[30] G. Chen, M. R. Kamaruzzaman, IEEE Int. Conf. Solid Dielectrics, **2007**, 510.
[31] C. C. Ku, R. Liepins, *Electrical Properties of Polymers: Chemical Principles*, Munich, New York, Hanser Publishers, **1987**.
[32] K. Yahagi, *IEEE Trans Electr Insul* **1980**, *EI-15*, 241.
[33] M. A. Bagirov, S. A. Abasov, V. P. Malin, A. Y. Jalilov, *J Appl Polym Sci* **1976**, *20*, 1069.
[34] M. E. Karlsson, X. Xu, H. Hillborg, V. Ström, M. S. Hedenqvist, F. Nilsson, R. T. Olsson, *RSC Adv* **2020**, *10*, 4698.
[35] F. Katzenberg, J. C. Tiller, *J Polym Sci B Polym Phys* **2016**, *54*, 1381.
[36] R. Hoeher, T. Raidt, C. Krumm, M. Meuris, F. Katzenberg, J. C. Tiller, *Macromol Chem Phys* **2013**, *214*, 2725.
[37] R. Hoeher, T. Raidt, M. Rose, F. Katzenberg, J. C. Tiller, *J Polym Sci B Polym Phys* **2013**, *51*, 1033.
[38] N. Guarrotxena, J. L. Millán, N. Vella, A. Toureille, *Polymer* **1997**, *38*, 4253.
[39] T. Raidt, R. Hoeher, F. Katzenberg, J. C. Tiller, *Macromol Rapid Commun* **2015**, *36*, 744.
[40] T. Raidt, R. Hoeher, F. Katzenberg, J. C. Tiller, *Macromol Mater Eng* **2017**, *302*, 1600308.
[41] H. Zhou, Dissertation, Blacksburg, Virginia, **1997**.
[42] Al-Shamrani, Abdoul Ali. Characterization, optimization and modelling of PE blends for pipe applications. Loughborough University. Thesis. **2010**. https://hdl.handle.net/2134/6019
[43] B. Vissouvanadin, S. Le Roy, G. Teyssedre, C. Laurent, I. Denizet, M. Mammeri, B. Poisson, Icpadm 2009: Proc. 9th Int. Conf. Properties and Applications of Dielectric Materials, **2009**, 961.
[44] N. Alberola, J. Y. Cavaille, J. Perez, *J Polym Sci B Polym Phys* **1990**, *28*, 569.
[45] H.-T. Liao, C.-S. Wu, *Polym-Plast Technol Eng* **2003**, *42*, 1.
[46] P. J. Flory, *Principles of Polymer Chemistry*, Cornell University Press, Ithaca **1953**.
[47] J. F. Lacoste, V. Bounor-Legaré, C. Joubert, M. F. Llauro, C. Monnet, P. Cassagnau, A. Michel, *Polymer* **2007**, *48*, 4615.
[48] P. T. Mather, X. Luo, I. A. Rousseau, *Annu Rev Mater Res* **2009**, *39*, 445.
[49] IEC/TS 62758: Calibration of space charge measuring equipment based on the pulsed electro-acoustic (PEA) measurement principle, **2012**.
[50] W.O. Statton, *J Polym Sci B Polym Lett Ed* **1973**, *11*, 211.
[51] S. Murakami, K. Senoo, S. Toki, S. Kohjiya, *Polymer* **2002**, *43*, 2117.

[52] D. Marsacq, P. Hourquebie, L. Olmedo, H. Janah, IEEE 1995 Annual Report - Conference on Electrical Insulation and Dielectric Phenomena, **1995**, 672.
[53] T. T. N. Vu, G. Teyssedre, L. Roy, C. Laurent, *IEEE Trans Dielectr Electr Insul* **2017**, *24*, 1405.
[54] C. W. B.: CIGRE Technical Brochure No. 496, **2012**.
[55] T. C. Zhou, G. Chen, R. J. Liao, Z. Q. Xu, *J Appl Phys* **2011**, *110*.
[56] T. J. LewisJ. P. Llewellyn, *J Appl Phys* **2013**, *113*.
[57] G. Chen, T. Y. G. Tay, A. E. Davies, Y. Tanaka, T. Takada, *IEEE Trans Dielectr Electr Insul* **2001**, *8*, 867.
[58] W. C. Du, W. Zhong, Y. J. Lin, L. Shen, Q. G. Du, *Eur Polym J* **2004**, *40*, 1987.
[59] E. A. Egorov, V. V. Zhizhenkov, *J Polym Sci Part B-Polym Phys* **1982**, *20*, 1089.
[60] C. F. Niedik, F. Jenau, F. Katzenberg, D. Segiet, Patent EP 3 795 331 A1, **2021**.

How to cite this article: C. F. Niedik, F. Jenau, M. Maricanov, D. Segiet, J. C. Tiller, F. Katzenberg, *Polym. Cryst.* **2021**, *4*(6), e10208. https://doi.org/10.1002/pcr2.10208